Fast Probabilistic 3-D Curvature Proprioception with a Magnetic Soft Sensor

Mason D. Mitchell, Forrest E. Hurley, and Cagdas D. Onal

***Abstract*— This paper introduces a cost-effective and high speed approach for predicting a 2-DOF bend parameterization for soft bodies through a magnetic and constant curvature system. We propose a design for a probabilistic particle filter that can be paired with magnetic simulations to produce highly accurate and fast pose information for parameter-constrained magnets. We include the design, fabrication, modeling, and experimental results of a physical sensor with the ability to produce both bend directionality and bend magnitude results with a speed of ∼60Hz. The proposed design consists of a magnet and tri-axis Hall effect sensor embedded in a soft silicone body. We demonstrate the effectiveness of this system through real-world interaction tests.**

I. Introduction

There are many techniques for proprioception in soft robotics, however there is not a standard for any application due to each technique's respective drawbacks. Optical fiber proprioception produces high quality results with quick update frequency, but these systems are often high in cost or equipment requirements [1]. Development and execution require complex custom circuits for optical fiber cable reading or high quality cameras with high refresh rate. Vision proprioception can also produce highly accurate results, however it usually requires expensive depth-sensing cameras and a hollow body for non-occluded sight to the vision targets [2]. Conversely, resistive bend sensors are low-cost and easy to manufacture, but the readings can result in drift over time and temperatures [3]. Capacitive sensors address many of these concerns [4]; unfortunately both resistive and capacitive modalities still affect the mechanical behaviour of the soft body in which they are mounted.

These drawbacks demonstrate that there is a need for a pose sensing option that offers real-time shape measurement without affecting the bending response of soft robotic structures. Our solution provides a probabilistic approach for predicting magnet pose in a parameterized body through the use of as little as one Hall Effect IC. One such example of this application is demonstrated in Figure 1. This figure shows the filter predicting the pose of a 2-degree-of-freedom (DOF) bending module. This prediction was done using a single embedded Hall Effect IC sensor and cuboid magnet.

This work was supported by the National Science Foundation (NSF) under an REU supplement for NSF Grant 1752195. Any opinions, findings, and conclusions or recommendations expressed in this material are those of the authors and do not necessarily reflect the views of the NSF.

Mason Mitchell & Cagdas Onal are with the WPI Soft Robotics Laboratory, Mechanical Engineering Department and Robotics Engineering Department at Worcester Polytechnic Institute. Forrest Eli Hurley is with the Mathematics Department at Georgia Institute of Technology. All correspondence should be addressed to Cagdas Onal cdonal@wpi.edu

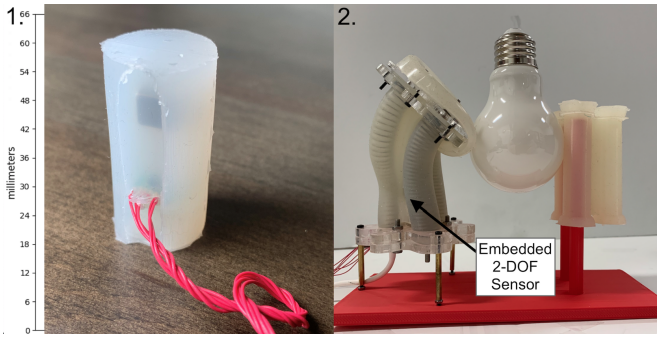

Fig. 1. **1.** Depicts sensor module components embedded in silicone cylinder created through a multi-step molding process. **2.** Shows a modified sensor module embedded in a soft 2-DOF module, able to handle delicate objects.

One advantage of embedded magnets for proprioception is that their presence minimally effects the properties of the surrounding material, as no sensor deformation is required for readings. The magnets can even be mounted where there is no physical connection between the electrical components and the body that requires sensing. These sorts of applications are already demonstrated in industry to robustly solve a multitude of rigid sensor tasks such as encoders and force sensors.

There is previous work utilizing magnets for pose estimation using a minimal number of Hall Effect sensors [5], [6]. These efforts employ mapping the entire workspace and using lookup tables for 1-DOF bend estimation. This process is unfortunately too slow for use in closed-loop control and would be reduced in speed exponentially for increased DOF applications.

One field that has heavily explored soft-bodied magnet proprioception is endoscopy [7], [8], [9], [10]. Endoscope research includes an impressive body of magnetic pose estimation work. However many methods proposed to predict the pose of the magnet utilize large arrays of Hall Effect sensors. Likewise, these solutions consist of highly complex algorithms designed to produce clear results in very controlled environments.

This paper introduces a novel probabilistic technique for 2-DOF applications that overcomes many of the drawbacks of these other systems. By implementing a single Hall Effect IC paired with a particle filter, this method allows for magnetic pose estimation in a multitude of applications for multi-DOF constraints. Particle filters provide several advantages over directly inverting the magnetic field equations. They do not generally require solving multidimensional nonlinear

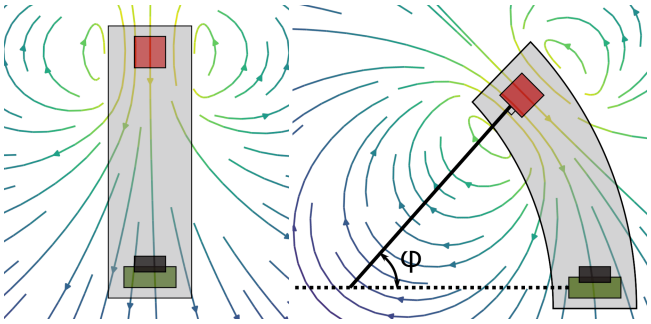

Fig. 2. Basic model of embedded magnet and Hall effect sensor in silicone cylinder at multiple positions. The magnetic flux field lines generated by the magnet are the same but interact differently with the sensor in different orientations. On the left is a silicone cylinder with bend angle 0; the right has a silicone cylinder with bend angle φ.

equations. Particle filters also inform their estimates based on recent history, improving stability. The computations represent a unique approach to magnetic pose estimation that can be applied to future tasks consisting of multiple magnetic components and sensors. These sets of magnet and sensor combinations could be arranged in a multitude of structures, such as a touch-sensitive plane, or a chain.

II. Modeling

We estimate the curvature of a soft body using an embedded Hall effect sensor and magnet. As the soft body bends, the relative locations and orientations of the magnet and Hall effect sensor change. This relative change then impacts the measured magnetic field as shown in Figure 2.

Unfortunately it is not easy to convert magnetic field strength measurements directly into a relative locations of the magnet and sensor. Although we focused on a soft body containing a single sensor-magnet pair, the calculations necessary to directly solve a chain of several interacting sensor-magnet pairs are nearly intractable. To sidestep this difficulty we use a particle filter linked to a magnetic field simulation.

A particle filter is a stochastic algorithm which operates on a set of particles each representing a possible state of a system [11], [12]. Each particle is associated with a single state within a given iteration of the algorithm. Kalman filters are closely related, being a special case optimization for linear Gaussian systems.

Particle filters use information from the recent past to improve the location estimate and to help describe the precision of the estimate. The past information or a priori belief about the true state of the system is incorporated through the initial distribution of particles at the beginning of each iteration. Each particle is assigned a probability based on how consistent it is with the measured magnetic field. The ensemble of particles is used to predict a single state and then the distribution of particles is updated to cancel out the particle probabilities. The result is the same as multiplying the particle distribution by the particle probability distribution and then normalizing.

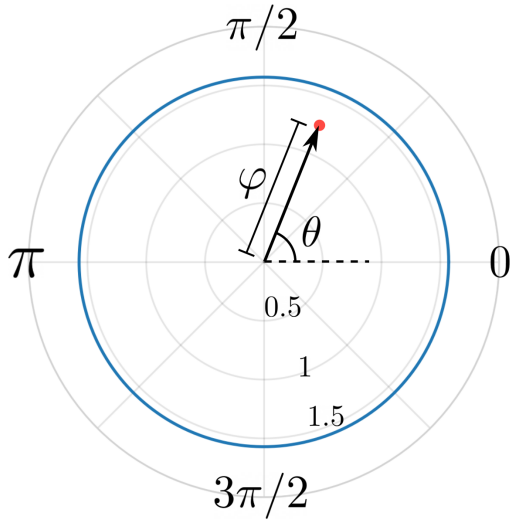

Fig. 3. A depiction of the parameter space containing all possible bend angle φ and direction θ combinations. The red dot represents one possible state.

The accuracy of the predicted location and the distributions is dependent on the number of particles in the filter, the correctness of the internal model, and noise. The number of particles in the filter can be decreased to reduce computational requirements at the cost of accuracy.

We assume that when bent, the soft body module has a constant curvature. We describe its state using two parameters: bend direction and bend angle. The bend angle φ is the angle of the soft body interpreted as an arc of a circle. The bend direction θ is the angle between the body projected into the XY plane and the X axis. The bend angle is bounded to be in the interval from 0 to $\pi/2$. Figure 3 contains a representation of the bend direction and bend angles in a parameter space. Each particle in the particle filter stores a state made up of these two parameters. The collection of particles in the particle filter represents a collection of possible states for the soft body module.

A. Weighting

There are several steps in the particle filter. The first is to assign weights to each particle. These weights or likelihoods represent an un-normalized probability of that particle's state being correct given the Hall effect sensor readings.

For each particle (using their states) a predicted magnetic field is calculated along with Hall effect sensor measurements [13], [14]. These simulated magnetic flux measurements are compared to the measurements from reality. Particles with modeled measurements closer to the experimental measurements have a higher likelihood. Let $\vec{x}$ be the predicted measurements, $\vec{y}$ be the actual measurements, and σ be a scaling constant. For simplicity we use a normal distribution for the likelihood function:

$$\mathcal{L}(\vec{x} \mid \vec{y}) = \exp\left(-\frac{||\vec{x}-\vec{y}||_2^2}{\sigma^2}\right). \quad (1)$$

After calculating the likelihoods, they are normalized to form weights which sum to 1. This step reduces numerical

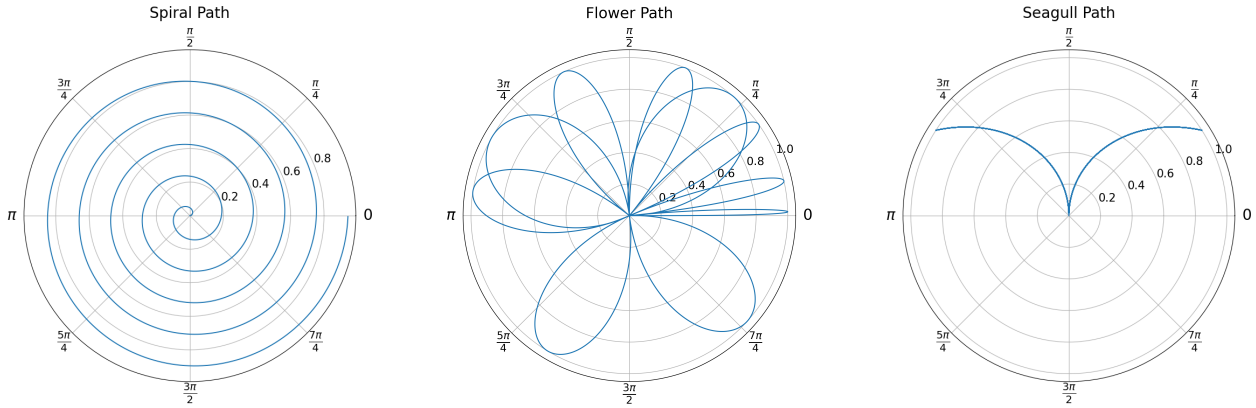

Fig. 4. Each path is defined by the parametric curves listed in Equations 5 (Spiral), 6 (Flower), and 7 (Seagull). Each equation is plotted in polar coordinates using bend direction as the angle and bend angle as the radius. For each equation, the maximum radius is 1 as to fully avoid the $\frac{\pi}{2}$ bound placed on bend angle.

errors in later steps, improves reliability, and allows the weights to be interpreted as probabilities. We calculate the sum of all of the particle likelihoods Z and then divide each likelihood by that sum. Both calculating and applying the normalization factor has to be handled carefully to avoid large numerical errors. We use a LogSumExp function to calculate Z. This normalization factor is applied to the likelihoods by subtracting inside the exponent:

$$\mathbb{P}(\vec{x} \mid \vec{y}) = \exp\left(-\frac{||\vec{x}-\vec{y}||_2^2}{\sigma^2} - \ln(Z)\right). \tag{2}$$

B. Predicting

After associating each potential particle with a probability, we calculate a single point estimate prediction. This prediction is our best guess of the true state based on the information contained in each of the particles.

We found that the point estimate was more accurate in simulation if it was only based on the 10 percent of particles with the highest probability. We took an average of the states of these high probability particles as the predicted state. The 10 percent cutoff worked sufficiently well for all of our tests.

Suppose that S is the set of states with the highest 10 percent of probabilities. Let θ_s, φ_s, and p_s be the bend direction, bend angle, and probability of a state $s \in S$. The predicted bend direction $\hat{\theta}$ and bend angle $\hat{\varphi}$ are

$$\hat{\theta} = \operatorname{atan2}\left(\sum_{s\in S}\sin(\theta_s), \sum_{s\in S}\cos(\theta_s)\right) \tag{3}$$

and

$$\hat{\varphi} = \frac{\sum_{s\in S}\varphi_s}{|S|}. \tag{4}$$

The bend angle $\hat{\varphi}$ must be between 0 and $\pi/2$, so a standard average is appropriate. However, because the bend direction $\hat{\theta}$ can be any angle, we use a circular mean to avoid boundary issues near 0 and 2π. We chose to use unweighted averages as we did not observe any further benefits from weighting states based on their probabilities.

C. Resampling

Resampling the particles is vital for exploring the state space and keeps the particle filter from becoming less efficient over time. The distribution of particle states is adjusted to incorporate the particle probabilities. Regions of the state space which have low probability given the sensor measurements lose particles, and high probability regions gain particles. After resampling, the distribution of particle states captures our belief about the state of the physical system given all current and past measurements.

Let N be the number of particles in the particle filter. Using random sampling with replacement, a new N particles are selected. The probability of any particle being selected in each of the N rounds is the probability from Equation 2. Some of the original particles will appear multiple times in the sample and some won't appear at all. A small amount of noise is then added to the states of the sampled particles; the noise separates duplicate particles and helps explore the state space.

When adding noise to the particle states it is desirable that bend direction can change more freely for states with a small bend angle φ. If bend angle is 0, the soft body is perfectly straight and all bend directions are equivalent. For small non-zero bend angles, a large change in bend direction only changes the magnet position and orientation slightly. This characteristic informed our choice of noise.

To add the noise each particle state is transformed into a vector. The bend direction θ is the direction of the state vector and its length is φ as shown in Figure 3. A random vector is drawn from a symmetric normal distribution with mean 0 and variance σ^2. The noise vector is added to the state vector. After adding the noise vector to the state vector, the result is transformed back into a bend direction and a bend angle based on its orientation and length. σ was equal to 0.02π in simulations and 0.002π for the experimental predictions.

Rejection sampling guarantees that the particle states remain valid. In particular, new random vectors are generated

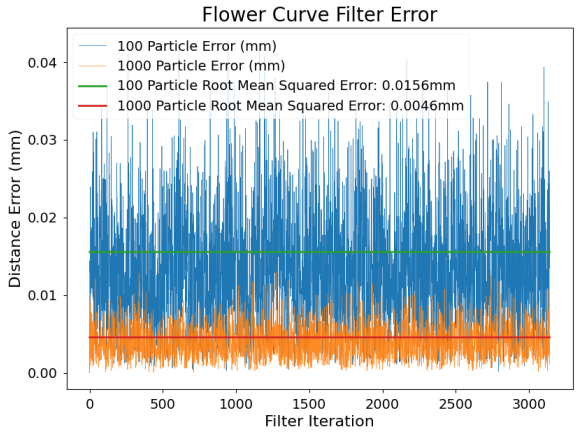

Fig. 5. Simulation results of position error using bend parameters from spiral input. This plot depicts the error of 100 and 1000 particle prediction. The error is the total 3D space between actual position and filter predicted position.

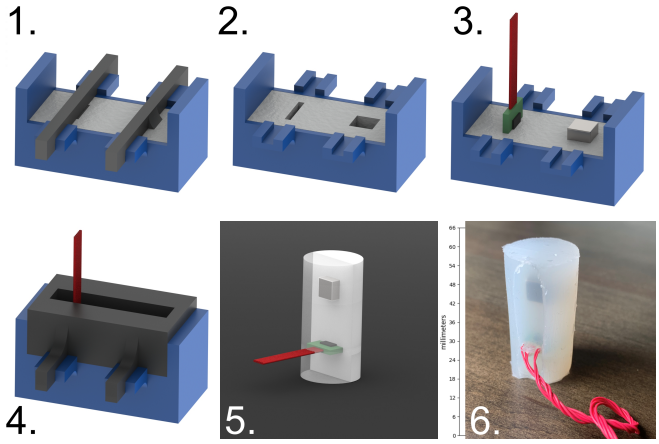

Fig. 6. **1.** Bottom mold with with silicone poured and component placeholder arms installed **2.** Placeholder arms removed after silicone sets, leaving press-fit insets for components **3.** Components (magnet and Hall effect sensor) fit into place inside silicone **4.** Top piece of mold added, and more silicone is poured to complete the sensor **5.** Sensor is removed from mold once set, ready for use **6.** Actual image of sensor plus scalebar after being fully constructed using the process described above.

until the resulting bend angle φ is no greater than $\pi/2$.

D. Model Results

To validate the filter we simulated several parametric curves

$$\theta = t, \qquad \varphi = 0.03t \tag{5}$$

$$\theta = (0.1t)^2, \qquad \varphi = \sin(t) \tag{6}$$

and

$$\theta = \sin(t) + \pi/2, \qquad \varphi = |\sin(t)|. \tag{7}$$

These Equations are labeled Spiral, Flower, and Seagull and are plotted in Figure 4.

The time t varied from 0 to 10π in increments of 0.01. At each time step a simulated sensor measurement was computed for each curve to drive particle filters with 1000 particles. To quantify the prediction error we compared the predicted positions of the magnet in Cartesian space with ground truth positions.

Figure 4 shows a plot of Equation 6 and Figure 5 shows the errors over the entire simulation period for that curve. Despite the drastic differences in the rate of change of the ground truth state at the beginning and end of this curve, the prediction errors are remarkably uniform. Although not shown here, the errors on the other two curves were similarly consistent. The predictions driven by Equations 5, 6, and 7 had root mean square errors of 0.0044 mm, 0.0046 mm, and 0.0046 mm respectively.

III. Fabrication & Design

A. Construction & Components

The proposed sensor was built using an embedded magnet and Hall Effect IC inside a soft cylinder. This design and corresponding components were chosen to promote constant curvature tendencies and reduce interference with the user.

- The low durometer silicone (Ecoflex 00-30) helps to give the module the necessary flexibility to cover a workspace large enough to be useful and reduces the effect of the sensor on any soft body that it would measure.
- The Hall Effect chip and corresponding IC was chosen for its accuracy, small size (.35in x .35in x .08in), and high speed interface enabled through SPI. The sensor (Melexis MLX90363) is embedded on a custom IC constructed through circuit etching in lab through a process identical to the one described in [15]. Due to concerns during the manufacturing process of excess movement inside the silicone, an acrylic (.4in x .4in x .0625in) plate was attached to the bottom of the IC with chemical adhesive to produce a larger surface area, discouraging shifting inside the silicone.
- The high-strength cuboid magnet (K&J Magnetics Part Number B444B) is chosen for its unique and strong magnetic field output. In contrast to a cylindrical shape, a cuboid magnet produces a more unique and less uniform magnetic field that proves helpful when applying localization techniques based on readings from a single point. The size of the magnet (.25in), and corresponding distance between the magnet and sensor (15mm, or $\sim$.6in) are picked to strike a balance between meaningful sensor length, low signal to noise ratio, and similarity in size to the Hall Effect IC.

Figure 6 shows the molding process utilized to construct the module with the components described. Overall, the sensor was effective in its performance and achieved its design goals.

IV. Experimental Results

As a demonstration of the applicability of the sensor, a secondary sensor module was constructed with a smaller silicone cylinder in order to fit inside an existing 2-DOF manipulator [16]. This sensor was used to measure the bend

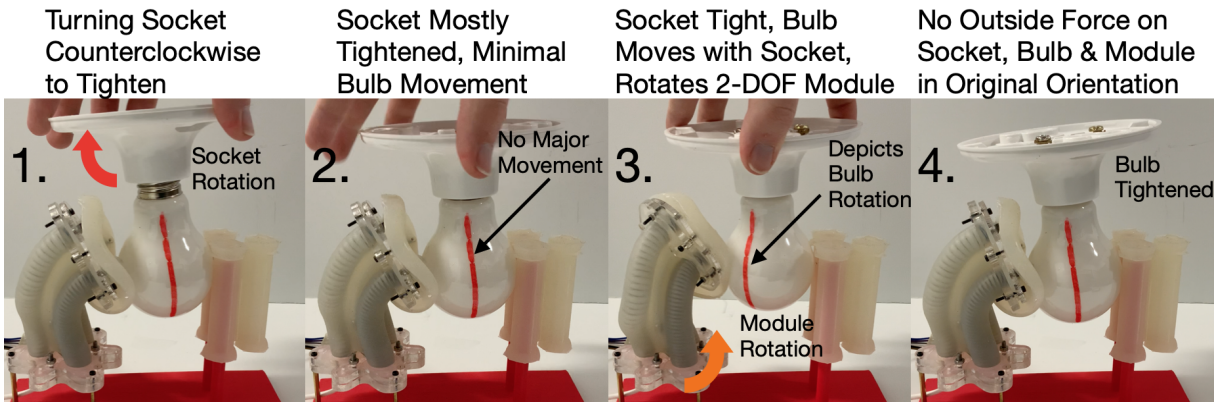

Fig. 7. Illustration of test performed to gather data in Figure 8. Same steps were repeated for all tests, to demonstrate repeatability of the results.

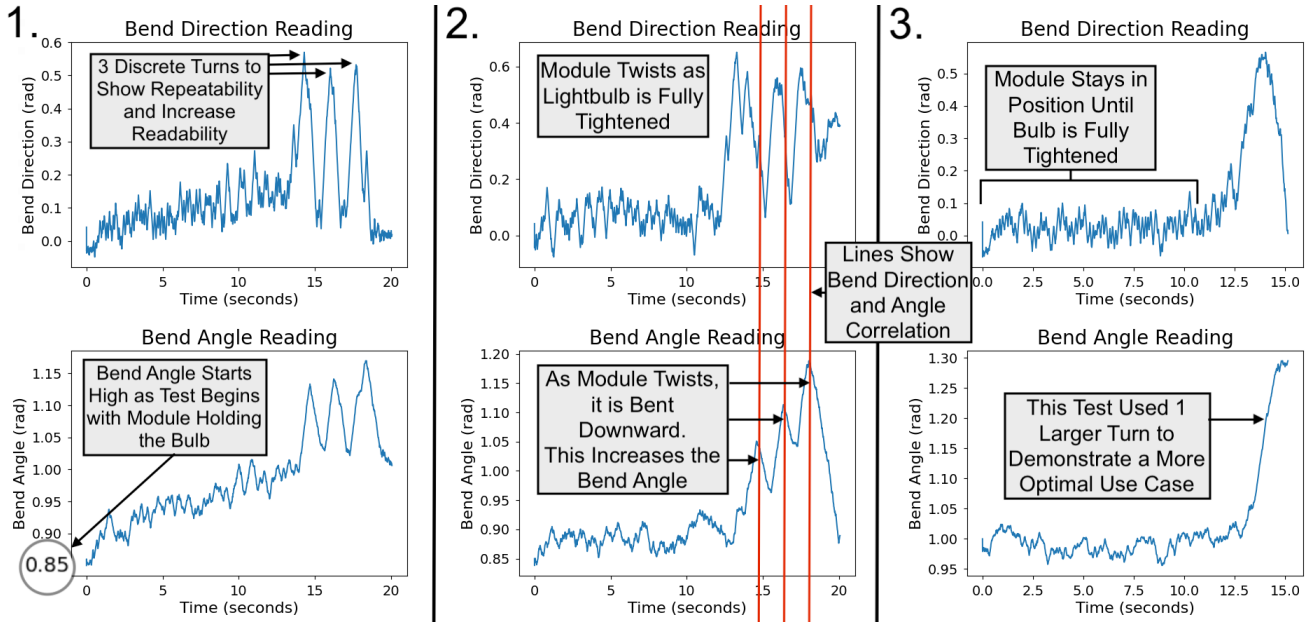

Fig. 8. Complete data of 3 independent lightbulb experiments. Vertical lines cross into plots taken from the same experiment. These lines show repeatable spikes when an attempt is made to tighten the lightbulb after it has been completely screwed in the socket. All experiments were run with 1000 particles, at 60Hz. **Experiment 1** (left) Demonstrates 3 attempts to further tighten the lightbulb. **Experiment 2** (middle) Also demonstrates 3 attempts to tighten the bulb more than possible. **Experiment 3** (right) Demonstrates a singular, much more concerted effort to tighten the bulb further than possible, which instigates a much more significant spike due the longer attempt. All three of these experiments show how this sensor is able to produce results accurate enough to interpret states in delicate tasks.

angle and direction parameters of the constant curvature manipulator at a speed of ∼60Hz.

A. *Lightbulb Test*

A task that is incredibly difficult in robotics, and slightly less so in soft robotics, is the handling of fragile objects. In this paper we utilize a 2-DOF module similar to the construction of the actuators in [5] to grasp a lightbulb. We can utilize the proprioceptive sensing enabled by the 2-DOF sensor to measure the bend angle and direction of the manipulator to determine when the bulb has completely tightened in its socket without excess force.

The experiment consists of a setup shown in Figure 7 with an active 2-DOF manipulator with an embedded sensor, and a static soft finger. Together, with pneumatic pressure used to bend the 2-DOF sensor, the lightbulb is held between the two points and a lightbulb socket is screwed in from the top manually.

Figure 8 shows the results and analysis of multiple repeated tests utilizing this process. The results demonstrate how this sensor is easily integrated into existing systems, and utilized for sensitive tasks that require high-speed, and consistent feedback.

B. *Motion Capture Demonstration*

To further validate our readings from our sensor, we placed the 2-DOF soft module in an Opti-Track motion capture environment to compare real measurements with our sensor measurements. We tracked the bend angle and direction of the 2-DOF soft module, as we increased and decreased the

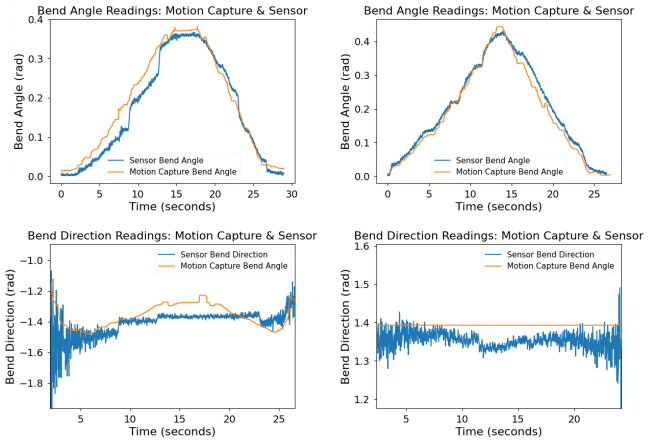

Fig. 9. Data from multiple bend tests, showing both bend direction and angle plots for motion capture ground truth and sensor readings. Offsets in data readings can be attributed to multiple factors other than sensor error, including imperfect placement in manufacturing and Opti-Track tracking errors.

pressure of different sets of chambers to produce varying levels of bending in multiple directions. Each experiment focused on bending in a singular direction, and slowly increasing and decreasing bend angle. Our results for this experiment can be seen in Figure 9.

V. Conclusions & Future Work

We introduce a method for pose estimation of a magnet in 3D space utilizing model-representative particle filter simulations. Our model can estimate the curvature of a soft body with a single Hall Effect sensor and magnet unlike many magnet pose estimating tools. We also evaluate the prediction quality on simulated data and test the filter on a physical manipulator. Our approach is able to identify when a light bulb was fully screwed in to its socket based on changes in a measured magnetic field.

The filter is expandable to countless scenarios. It could be applied to non constant-curvature settings or multiple magnets and sensors could be incorporated in a single device. Having multiple magnets and sensors would allow for multiple-point localization within the same body. There is plenty of room for the particle filter to be made more efficient and accurate through algorithmic improvements. Other than improving the filter or applying it to more complex scenarios, there is also room for improvement in the empirical evaluation of its accuracy. Tracking a physical manipulator with a motion capture system while collecting the magnetic field data from a calibrated sensor is an important future step in measuring the real world accuracy of the filter.

Python code for reproducing the results in this paper is available in a public repository[1].

Acknowledgments

The authors thank Erik Skorina from the Robotics Engineering Department at WPI for their assistance with 3D printing, as well as impactful experimental and research advice.

[1]https://github.com/MasonDMitchell/pose-chain/tree/master

References

[1] Qi Wang, and Yu Liu, "Review of optical fiber bending/curvature sensor," in *Measurement,* vol. 130, pp. 161-176, 2018.

[2] R. Wang, S. Wang, S. Du, E. Xiao, W. Yuan and C. Feng, "Real-Time Soft Body 3D Proprioception via Deep Vision-Based Sensing," in *IEEE Robotics and Automation Letters,* vol. 5, no. 2, pp. 3382-3389, April 2020.

[3] G. Saggio, A. Lagati, G. Orengo, "Shaping Resistive Bend Sensors to Enhance Readout Linearity" in *ISRN Electronics,* pp. 359759, November 2012.

[4] A. Sreejan and Y. Shivraj, "A Review on Applications of Flex Sensors," in *International Journal of Emerging Technology and Advanced Engineering*, vol. 7, pp. 97-100, 2017.

[5] M. Luo, E. H. Skorina, W. Tao, F. Chen, S. Ozel, Y. Sun, and C. D. Onal, "Toward Modular Soft Robotics: Proprioceptive Curvature Sensing and Sliding-Mode Control of Soft Bidirectional Bending Modules," in *Soft Robotics*, pp. 117-125, June 2017.

[6] S. Ozel, N. A. Keskin, D. Khea, C. D. Onal, "A precise embedded curvature sensor module for soft-bodied robots," in *Sensors and Actuators A: Physical,* vol. 236, pp. 349-356, 2015.

[7] J. Edelmann, A. Petruska, and B. Nelson, "Estimation-Based Control of a Magnetic Endoscope without Device Localization," in *J. Medical Robotics Res*, vol. 3, 2018.

[8] K. M. Miller, A. W. Mahoney, T. Schmid and J. J. Abbott, "Proprioceptive magnetic-field sensing for closed-loop control of magnetic capsule endoscopes," in *IEEE/RSJ International Conference on Intelligent Robots and Systems Vilamoura-Algarve, Portugal, 2012,* pp. 1994-1999, 2012.

[9] T. D. Than, G. Alici, H. Zhou, and W. Li, "A review of localization systems for robotic endoscopic capsules," in *IEEE Transactions on Biomedical Engineering,* vol. 59, no. 9, pp. 2387-2399, Sept. 2012.

[10] C. Hu, M. Li, S. Song, W. Yang, R. Zhang and M. Q. H. Meng, "A Cubic 3-Axis Magnetic Sensor Array for Wirelessly Tracking Magnet Position and Orientation," in *IEEE Sensors Journal,* vol. 10, no. 5, pp. 903-913, May 2010.

[11] J. Elfring, E. Torta, and R. van de Molengraft, "Particle filters: A hands-on tutorial," *Sensors (Switzerland)*, vol. 21, no. 2, pp. 438, Jan. 2021.

[12] N. J. Gordon, D. J. Salmond, and A. F. M. Smith, "Novel approach to nonlinear/non-Gaussian Bayesian state estimation," in *IEE Proceedings,* vol. 140, no. 2, pp. 107–113, Apr. 1993.

[13] M. Ortner, and L. G. C. Bandeira, "Magpylib: A free Python package for magnetic field computation," in *SoftwareX,* vol. 11, pp. 100466, 2020.

[14] J. M. Camacho and V. Sosa, "Alternative method to calculate the magnetic field of permanent magnets with azimuthal symmetry," in *Revista mexicana de física,* pp. 8-17, 2013.

[15] A. Dwivedi, A. Ramakrishnan, A. Reddy, K. Patel, S. Ozel and C. D. Onal, "Design, Modeling, and Validation of a Soft Magnetic 3-D Force Sensor," in *IEEE Sensors Journal,* vol. 18, no. 9, pp. 3852-3863, 1 May, 2018.

[16] Y. Qin, Z. Wan, Y. Sun, E. H. Skorina, M. Luo and C. D. Onal, "Design, fabrication and experimental analysis of a 3-D soft robotic snake," *2018 IEEE International Conference on Soft Robotics (RoboSoft),* pp. 77-82, 2018.